Available online at www.sciencedirect.com
SCIENCE DIRECT®
Acta Materialia 53 (2005) 5313–5321
Acta MATERIALIA
www.actamat-journals.com

Phase-field simulation of polarization switching and domain evolution in ferroelectric polycrystals

S. Choudhury [a,*], Y.L. Li [a], C.E. Krill III [b], L.-Q. Chen [a]

[a] *Department of Materials Science and Engineering, Pennsylvania State University, University Park, 305 Steidle Building, PA 16803, United States*
[b] *Materials Division, University of Ulm, Albert-Einstein-Allee 47, D-89081 Ulm, Germany*

Received 4 March 2005; received in revised form 28 July 2005; accepted 29 July 2005
Available online 21 September 2005

Abstract

A phase-field model is developed for predicting the polarization switching and domain structure evolution under an applied electric field in ferroelectric polycrystals. The model takes into account realistic grain structures as well as various energetic contributions, including elastic energy, electrostatic energy, and domain wall energy. A hysteresis loop – average polarization as a function of applied electric field – is computed, and the detailed domain evolution process during switching is analyzed. In particular, the role of grain boundaries in the nucleation and growth of new domains is studied. It is shown that switching takes place through the nucleation of 90° domains at grain boundaries and subsequent growth into the grain interiors instead of direct 180° domain switching. A correlation between the domain structures in neighboring grains was observed, and polarization switching in one grain was found to affect the switching in neighboring grains.

Keywords: Phase-field models; Ceramics; Ferroelectricity; Domain switching

1. Introduction

Ferroelectric ceramics are of considerable interest due to their applications in various electronic, microelectronic and electrooptical devices [1], such as acoustic sensors and actuators [2]. In microelectronics, the switching behavior of ferroelectrics under an applied electric field is exploited in the design of nonvolatile random access memories. Switching involves the nucleation of new domains and domain wall motion under an applied electric field. Therefore, the ability to predict domain evolution under an applied field is crucial to the development of a fundamental understanding of polarization switching mechanisms.

The most studied, and perhaps also the simplest, case is 180° domain switching in single crystals [3]. In a single crystal, 180° polarization switching is generally thought to proceed by the nucleation of antiparallel domains and subsequent growth via domain wall migration [3,4]. In the high-field regime, it is believed that nucleation occurs more rapidly, and switching is completed by domain wall migration [5], until collision of domains takes place [6]. For both single-crystal bulk and thin-film systems [7–10], a number of computer simulations have been carried out of domain evolution during ferroelectric transitions as well as domain evolution under an applied field. However, switching involving both 180° and

* Corresponding author. Tel.: +1 814 865 0389.
E-mail address: sxc398@psu.edu (S. Choudhury).

1359-6454/$30.00
doi:10.1016/j.actamat.2005.07.040

90° domain walls occurring in polycrystals is less well understood, although there have been several theoretical studies of the switching behavior of ferroelectric polycrystals [11–15].

Prior models typically assumed that ferroelectric polycrystals are made up of an array of single-domain grains, and the ferroelectric or ferroelastic switching occurs when the energy provided by the applied field exceeds a critical value [11]. The polarization vs. applied electric field (P–E) loops predicted by such an approach display the main features of those obtained experimentally. An alternative approach is the finite element method of Hwang et al. [12] based on similar switching criteria, which finds that switching in a given grain is inhibited by the presence of neighboring grains. Arlt [13] proposed a different model for predicting domain switching mechanism in ferroelectric polycrystal. The model is based on the nucleation of a temporary domain wall by overcoming a certain energy barrier in order to adjust the elastic energy associated by the formation of wall. Recently, Zhang et al. [14,15] presented a computational model for domain switching in single-crystal and bicrystal ferroelectrics. Through 2D simulations, it was shown that ferroelectric domain switching behavior changes in the bicrystal as the difference in crystallographic orientation between the grains increases.

In this paper, we describe a 3D phase-field model for studying the domain evolution in a ferroelectric polycrystal under an applied electric field, similar to phase-field models for martensitic transformations in polycrystals [16]. Previously, the phase-field approach has been employed to investigate the microstructure evolution during solidification [17] and a variety of solid-state phase transformations [18]. We studied the temporal evolution of domain structures during polarization switching in a ferroelectric polycrystal using $PbTiO_3$ as a model system. It is well known that in a real $PbTiO_3$ polycrystal, the stress induced by the ferroelectric phase transition is so large that it causes cracks to form. The possibility of such crack formation is neglected in the simulations. Since the model is rather computationally intensive in three-dimensions (3D), as a first attempt we conducted our simulations in two-dimensions (2D). Owing to this 2D nature and neglect of the possibility of crack formation, the focus of this paper is on the mechanisms for domain switching and the various energetic contributions to the switching process, rather than on a quantitative comparison with experimentally measured hysteresis loops.

2. Phase-field model of ferroelectric domain structures in polycrystals

To describe the domain structures in polycrystals, there are two levels of structures, i.e., the grain structure and the domain structure in each individual grain. We employed the phase-field model for grain growth to generate 2D and 3D grain structures [19]. The domain structure within each grain is described by the inhomogeneous distribution of the local polarization P_i^L, where $i = 1, 2, 3$, and the superscript L indicates that the polarization components are expressed in local coordinates within each individual grain. The total free energy of a ferroelectric polycrystal is given by

$$F = \int_V (f_{\text{bulk}} + f_{\text{elas}} + f_{\text{grad}} + f_{\text{elec}})\, \mathrm{d}V, \tag{1}$$

where f_{bulk} denotes the bulk free energy density, f_{elas} the elastic energy density, f_{grad} the gradient energy density (nonzero only near domain walls and grain boundaries), and f_{elec} the electrostatic energy density.

The bulk free energy density in a given grain is expanded in terms of polarization components using the Landau theory, i.e.,

$$\begin{aligned} f_{\text{bulk}} = {} & \alpha_1[(P_1^L)^2 + (P_2^L)^2 + (P_3^L)^2] + \alpha_{11}[(P_1^L)^4 \\ & + (P_2^L)^4 + (P_3^L)^4] + \alpha_{12}[(P_1^L P_2^L)^2 + (P_2^L P_3^L)^2 \\ & + (P_3^L P_1^L)^2] + \alpha_{111}[(P_1^L)^6 + (P_2^L)^6 + (P_3^L)^6] \\ & + \alpha_{112}[(P_1^L)^2\{(P_2^L)^4 + (P_3^L)^4\} + (P_2^L)^2\{(P_3^L)^4 \\ & + (P_1^L)^4\} + (P_3^L)^2\{(P_1^L)^4 + (P_2^L)^4\}] \\ & + \alpha_{123}(P_1^L P_2^L P_3^L)^2, \end{aligned} \tag{2}$$

where α_1, α_{11}, α_{12}, α_{111}, α_{112}, α_{123} are the dielectric stiffness and higher-order stiffness coefficients under stress-free boundary conditions [20], and P_1^L, P_2^L, P_3^L are the polarization components in the local crystallographic coordinate system within each grain.

In order to solve the elasticity and electrostatic equations, we introduce a common global coordinate system for all grains. We describe the orientation of a particular grain in the polycrystalline structure using three Euler angles (φ, θ, ψ) [21], corresponding to three consecutive counter-clockwise rotations with respect to the global coordinates (x_1, x_2, x_3): φ about the x_3-axis, θ about the rotated x_1'-axis and ψ about the newest x_3'-axis. Accordingly, the transformation matrix from the global to local coordinate system is given by

$$tr = \begin{pmatrix} \cos[\varphi]\cos[\psi] - \cos[\theta]\sin[\varphi]\sin[\psi] & \sin[\varphi]\cos[\psi] + \cos[\theta]\cos[\varphi]\sin[\psi] & \sin[\theta]\sin[\psi] \\ -\cos[\theta]\cos[\psi]\sin[\varphi] - \cos[\varphi]\sin[\psi] & \cos[\theta]\cos[\varphi]\cos[\psi] - \sin[\varphi]\sin[\psi] & \sin[\theta]\cos[\psi] \\ \sin[\theta]\sin[\varphi] & -\cos[\varphi]\sin[\theta] & \cos[\theta] \end{pmatrix}. \tag{3}$$

The polarization in the local coordinate system, P_i^L, is related to that in the global system, P_i, through

$$P_i^L = tr_{ij} P_j, \tag{4}$$

where tr_{ij} represents the ij-component of the transformation matrix tr. The local polarization is unique to a particular grain and assumed to remain constant during domain evolution.

The elastic energy density is given by

$$f_{\text{elas}} = \frac{1}{2} C_{ijkl} e_{ij} e_{kl} = \frac{1}{2} C_{ijkl} (\varepsilon_{ij} - \varepsilon_{ij}^0)(\varepsilon_{kl} - \varepsilon_{kl}^0), \tag{5}$$

where C_{ijkl} represents the elastic stiffness tensor, and e_{ij}, ε_{ij} and ε_{ij}^0 denote the elastic strain, total strain and spontaneous strain, respectively. The spontaneous strain in a given grain can be expressed with respect to the local coordinate system by $\varepsilon_{ij}^{0L} = Q_{ijkl} P_k^L P_l^L$, where Q_{ijkl} is the electrostrictive coefficient of the corresponding single crystal. Therefore, the spontaneous strain in the global coordinate system can be obtained from

$$\varepsilon_{ij}^0 = tr_{ki}\ tr_{lj} \varepsilon_{kl}^{0L}. \tag{6}$$

The total strain ε_{ij} can be written as the sum of the spatially independent homogenous strain, $\overline{\varepsilon}_{ij}$, and a spatially dependent heterogeneous strain, $\delta\varepsilon_{ij}$, i.e.,

$$\varepsilon_{ij} = \overline{\varepsilon}_{ij} + \delta\varepsilon_{ij}. \tag{7}$$

The homogenous strain determines the macroscopic shape deformation of the entire polycrystal resulting from an applied strain, phase transformations or domain structure changes. If the external boundary of the polycrystal is clamped, $\overline{\varepsilon}_{ij}$ is zero. The heterogeneous strain is defined in such a way that $\int_V \delta\varepsilon_{ij}\, \mathrm{d}V = 0$.

To solve the equilibrium heterogeneous strain field $\delta\varepsilon_{ij}$, we introduce a set of displacements $u_i(\boldsymbol{x})$, such that $\delta\varepsilon_{ij} = 1/2(u_{i,j} + u_{j,i})$, with $u_{i,j} = \partial u_i/\partial x_j$. The mechanical equilibrium condition is given by $\sigma_{ij,j} = 0$, where σ_{ij} is the elastic stress, and $\sigma_{ij,j}$ is the sum of the derivatives of σ_{ij} with respect to x_1, x_2 and x_3 respectively $\sigma_{ij} = C_{ijkl} e_{kl} = C_{ijkl}(\varepsilon_{kl} - \varepsilon_{kl}^0)$. For simplicity, we assume that the elastic modulus is isotropic and homogeneous and thus $C_{ijkl} u_{k,lj} = C_{ijkl} \varepsilon_{kl,j}^0$. The equilibrium displacement and the heterogeneous strain components can be solved using Fourier transforms [22].

The contribution of the domain walls to the total free energy, i.e., the domain wall energy – is introduced through the gradient of the global polarization field. For the sake of simplicity and because of a dearth of experimental values for the domain wall energies along different directions, we assume the wall energy to be isotropic. For an isotropic domain wall energy, the gradient energy density can be written as

$$\begin{aligned} f_{\text{grad}} = \frac{1}{2} G_{11} [&(P_{1,1})^2 + (P_{1,2})^2 + (P_{1,3})^2 + (P_{2,1})^2 + (P_{2,2})^2 \\ &+ (P_{2,3})^2 + (P_{3,1})^2 + (P_{3,2})^2 + (P_{3,3})^2], \end{aligned} \tag{8}$$

where G_{11} is the gradient energy coefficient and $P_{i,j} = \partial P_i/\partial x_j$ denotes the spatial differentiation of the polarization components.

Under an applied electric field, the electrical energy density f_{elec} is comprised of the dipole–dipole interaction energy density due to the inhomogeneous distribution of polarization, f_{dipole}; the depolarization energy density due to surfaces, f_{depol}; and the energy density due to the applied electric field, f_{appel}:

$$f_{\text{elec}} = f_{\text{dipole}} + f_{\text{depol}} + f_{\text{appel}}. \tag{9}$$

For an electrically inhomogeneous system the long-range electric dipole–dipole interaction energy density is given by

$$f_{\text{dipole}} = -\frac{1}{2} E_i P_i, \tag{10}$$

where E_i denotes the inhomogeneous electric field due to dipole–dipole interactions. It is obtained by solving the electrostatic equilibrium equation given by $D_{i,i} = 0$, where D_i is the electrical displacement represented by $D_i = \varepsilon_0 \kappa_{ij} E_j + P_i$, where $\varepsilon_0 = 8.85 \times 10^{-12}\ \mathrm{Fm}^{-1}$ represents the dielectric permittivity of vacuum and κ_{ij} the relative dielectric permittivity, assumed to be independent of space [23]. Spatially differentiating the electric displacement and using the electrostatic equilibrium equation, we find

$$D_{i,i} = 0 = \varepsilon_0 (\kappa_{ij} E_{j,i}) + P_{i,i}. \tag{11}$$

The electric field E_i is related to the electric potential ϕ through $-\phi_{,i} = E_i$. Hence, by assuming $\kappa_{ij} = 0$ for $i \neq j$ and rearranging the terms in Eq. (11), we obtain

$$(\kappa_{11}\phi_{,11} + \kappa_{22}\phi_{,22} + \kappa_{33}\phi_{,33}) = \frac{1}{\varepsilon_0}(P_{1,1} + P_{2,2} + P_{3,3}). \tag{12}$$

Transforming Eq. (12) to Fourier space yields

$$\phi(\boldsymbol{\zeta}) = -\frac{1}{\varepsilon_0} \frac{I(\zeta_1 P_1(\boldsymbol{\zeta}) + \zeta_2 P_2(\boldsymbol{\zeta}) + \zeta_3 P_3(\boldsymbol{\zeta}))}{(\kappa_{11}\zeta_1^2 + \kappa_{22}\zeta_2^2 + \kappa_{33}\zeta_3^2)}, \tag{13}$$

where ζ_i is the component of positional co-ordinate $\boldsymbol{\zeta}$ in the Fourier space, and $I = \sqrt{-1}$. The symbols $\phi(\boldsymbol{\zeta})$ and $P_i(\boldsymbol{\zeta})$ denote the Fourier transforms of the electric potential and polarization component, respectively, and are given by

$$\begin{aligned} P_i(\boldsymbol{\zeta}) &= \frac{1}{(2\pi)^3} \int \int_{-\infty}^{\infty} \int P_i(\boldsymbol{x}) \mathrm{e}^{-\mathrm{I}\boldsymbol{x}.\boldsymbol{\zeta}}\, \mathrm{d}^3 x, \\ \phi_i(\boldsymbol{\zeta}) &= \frac{1}{(2\pi)^3} \int \int_{-\infty}^{\infty} \int \phi_i(\boldsymbol{x}) \mathrm{e}^{-\mathrm{I}\boldsymbol{x}.\boldsymbol{\zeta}}\, \mathrm{d}^3 x. \end{aligned} \tag{14}$$

The electric field and electric potential are related by $E_i(\boldsymbol{\zeta}) = -I\zeta_i \phi(\boldsymbol{\zeta})$. Therefore, the real-space electric field arising from dipole–dipole interactions is given by

$$E_i(\boldsymbol{x}) = \int \int_{-\infty}^{\infty} \int E_i(\boldsymbol{\zeta}) \mathrm{e}^{\mathrm{I}\boldsymbol{x}.\boldsymbol{\zeta}}\, \mathrm{d}^3 \zeta. \tag{15}$$

It should be noted that the point $\zeta = 0$ is excluded when calculating the dipole–dipole interaction energy. The average depolarization field in global coordinates due to the presence of surface charges can be approximated as

$$E_{i,\text{depol}} = -\frac{1}{\varepsilon_i}\overline{P_i}, \tag{16}$$

where $\overline{P_i}$ is the spatial average of the ith component of polarization, and $\varepsilon_i = \varepsilon_0\kappa_{ii}$ (no summation implied by the repeated index). Hence, the depolarization energy density is

$$f_{\text{depol}} = -\frac{1}{2}E_{i,\text{depol}}\overline{P_i}. \tag{17}$$

Finally, when an externally electric field $E_{i,\text{appel}}$ is applied in the global ith direction, an additional contribution f_{appel} should be taken into consideration:

$$f_{\text{appel}} = -E_{i,\text{appel}}\overline{P_i}. \tag{18}$$

With the total free energy F expressed as a functional of the global polarization, the temporal evolution of the domain structure can be obtained by solving the time-dependent Ginzburg–Landau (TDGL) equation

$$\frac{\partial P_i(\boldsymbol{x},t)}{\partial t} = -M\frac{\delta F}{\delta P_i(\boldsymbol{x},t)}, \quad i = 1,2,3, \tag{19}$$

where M is a kinetic coefficient related to the domain mobility, and t is time.

3. Numerical simulations

Although the model described in the last section is applicable to 3D polycrystalline systems, for computational reasons and simplicity we performed 2D simulations to study the qualitative features and mechanisms of domain evolution during polarization switching in polycrystalline ferroelectrics. We generated a 2D grain structure employing the grain-growth model developed by Krill and Chen [19]. Fig. 1 shows an example of a 2D grain structure generated by the 2D version of the 3D grain-growth model. In this work, we assume that the grain structure is static, i.e., it does not evolve with time. The simulated polycrystal is comprised of 91 grains, with each grain assumed to be oriented along a different crystallographic direction. In 2D the orientations of different grains can be specified by the rotation angle φ about the x_3-axis; hence, the angles θ and ψ are assumed to be zero in Eq. (3). The grain orientations vary between 0° and 45° because of symmetry. The orientation of each individual grain (φ) was assigned randomly and does not change with time during domain switching.

The temporal evolution of the global polarization vector fields are obtained by numerically solving

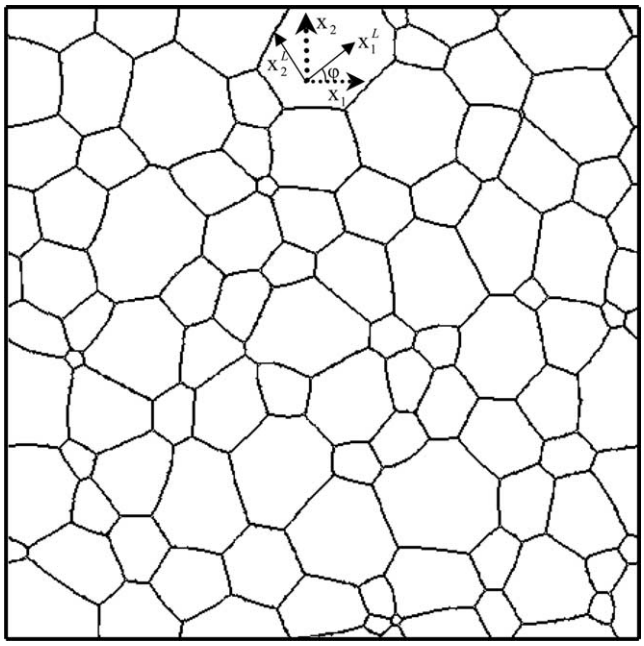

Fig. 1. Grain structure generated using the 2D phase-field model for grain growth. The dotted and solid pairs of arrows illustrate the global and local coordinate systems, respectively, with $0° \leqslant \varphi \leqslant 45°$.

Eq. (19) using the semi-implicit Fourier spectral method [24]. The Landau energy coefficients in Eq. (2) and the electrostrictive coefficients for $PbTiO_3$ are found in [10,20] and were given originally by Haun et al. [25]. In the simulations we employed 512×512 discrete grid points and periodic boundary conditions applied along the x_1 and x_2 axes. The grid spacing was chosen to be $\Delta x_1 = \Delta x_2 = l_0$, where $l_0 = \sqrt{G_{110}/\alpha_0}$ and $\alpha_0 = |\alpha_1|_{T=25\,^\circ\text{C}}$. We assumed that the gradient energy coefficient is $G_{11}/G_{110} = 0.6$. The corresponding domain wall width is about $1.5\Delta x_1$, and the domain wall energy densities at $T = 25\,^\circ\text{C}$ are evaluated to be about $0.60\alpha_0 l_0 P_0^2$ for 90° domain walls and $1.26\alpha_0 l_0 P_0^2$ for 180° domain walls. The spontaneous polarization is $P_0 = |P|_{T=25\,^\circ\text{C}} = 0.757\ \text{Cm}^{-2}$. If $l_0 = 2.0$ nm, $G_{110} = 7.12 \times 10^{-10}\ \text{C}^{-2}\ \text{m}^4\ \text{N}$. The corresponding specific domain wall energy is about $0.12\ \text{Jm}^{-2}$ for 90° domain walls, and the wall width is around 3.0 nm, which is similar to experimentally observed domain wall energies and widths in single crystals [26]. With $l_0 = 2.0$ nm, the average grain radius in the simulated grain structure in Fig. 1 is about 110 nm. The time step in Eq. (19) is taken to be $\Delta t/t_0 = 0.05$, where $t_0 = 1/(\alpha_0 M)$. For the calculation of elastic energy, we took the elastic constants to be isotopic and homogeneous, with shear modulus $\mu = 0.476 \times 10^{11}\ \text{Nm}^{-2}$ and Poisson's ratio $\nu = 0.312$, in order to avoid having to solve inhomogeneous elastic equations in a polycrystal. Clamped boundary conditions were used. For the dipole–dipole interaction energy calculations, we used $\kappa_{11} = \kappa_{22} = 100$ in our simulation.

A domain structure was first generated by performing the simulations without an applied electric field, starting from an initial paraelectric state with small random perturbations. A depolarizing field was assumed to exist along both x_1 and x_2 directions. To compute the PE loop, an electric field is applied to the generated domain structure in the x_1 direction, while a depolarizing field is assumed to exist along the x_2 direction. At each increment of the electric field, the domain structure from the previous simulation is used as the starting configuration.

4. Results

Fig. 2 shows an example of the domain structure in a polycrystal at zero applied electric field following 50,000 iterations beginning from a paraelectric state. There are four tetragonal variants, labeled as a_1 positive, a_2 positive, a_1 negative, and a_2 negative, with polarization components $(P_1^L > 0, P_2^L = P_3^L = 0)$, $(P_2^L > 0, P_1^L = P_3^L = 0)$, $(P_1^L < 0, P_2^L = P_3^L = 0)$ and $(P_2^L < 0, P_1^L = P_3^L = 0)$, respectively. The four variants are represented by different shading. As expected, the polarization directions for the domains vary from one grain to another, with both 90° and 180° domain walls existing in the simulation cell. Fig. 3 shows the $\overline{P_1}$ vs. $E_{1,\text{appel}}$ loop (PE loop) as an electric field is applied along the x_1 direction. Each point in the PE loop represents the average polarization at the end of 5000 iterations at the given electric field. As the applied electric field increases, the volume fractions of the tetragonal a_1 and a_2 domains change. The polarization directions in different grains try to orient along the direction of the electric field. Therefore, for the maximum positive applied electric field, corresponding to point b in Fig. 3, the a_1 domains with negative polarization vanish, as seen in Fig. 4. The domain structure is predominantly comprised of just two types of domains – namely, a_1 positive and a_2 negative. A small volume fraction of a_2 positive domains is present in the grains having an orientation close to that of the applied field.

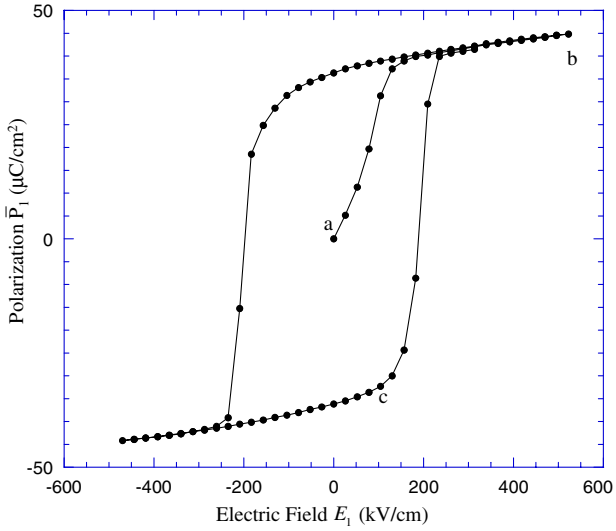

Fig. 3. Hysteresis loop computed for lead titanate ceramic.

To illustrate the domain evolution process in more detail, we plot in Fig. 5(i)–(iv) the evolution of the polarization configurations within the dotted rectangular box of Fig. 2 for various iteration numbers N_{itr} at

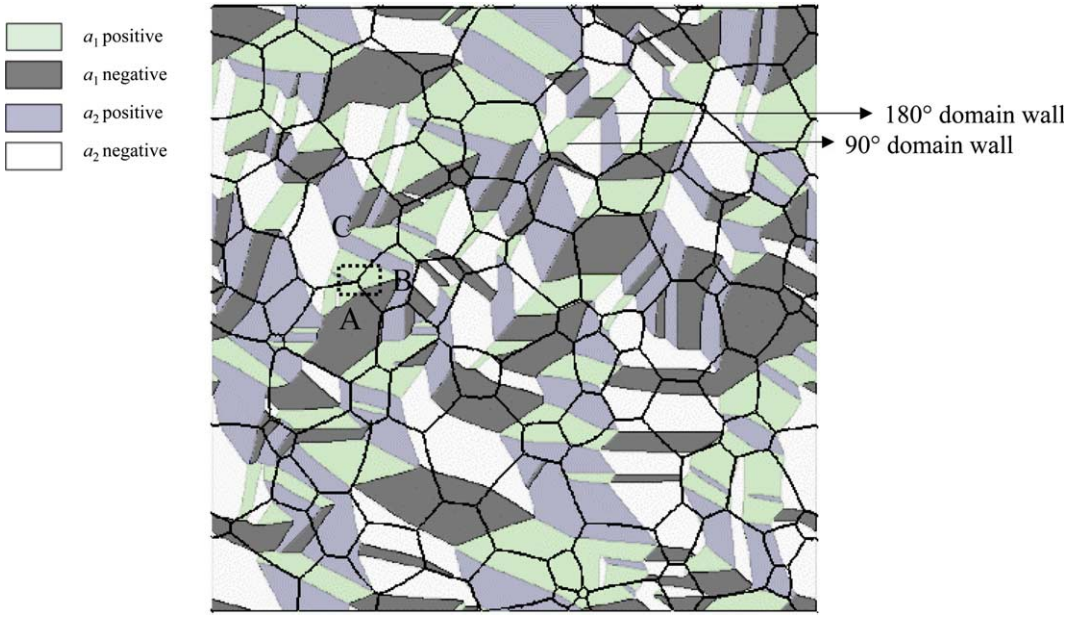

Fig. 2. Domain structure after 50,000 iterations without applied electric field. The four tetragonal variants are shaded according to the legend at top left.

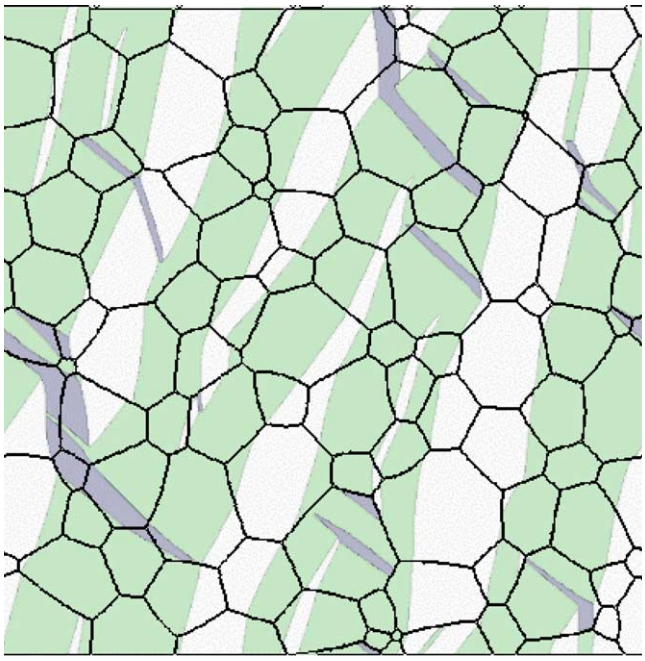

Fig. 4. Domain structure corresponding to the point b in the PE loop of Fig. 3. The tetragonal a_1 negative variant is completely absent, and the majority of the simulation cell is comprised of two tetragonal variants.

point c of Fig. 3, where $E_{1,\text{appel}} = 104.48$ kV/cm. The small arrows in Fig. 5 indicate the local polarization direction. Fig. 5(i) shows the domain structure in grain A after the first iteration. As the number of iterations increases, an a_1 domain with positive polarization nucleates at the grain boundary where the twin boundary and the grain boundary meet (Fig. 5(ii)). A solid circle marks the location of the nucleated domain. The domain then grows towards the center of grain A, with the large arrow in Fig. 5(ii) indicating the direction of domain growth. From Fig. 5(iii) it is evident that switching in grain A propagates to the neighboring grain B, resulting in the nucleation a new domain in grain B. The nucleated domain then grows toward the center of grain B, as shown in Fig. 5(iv). Switching occurs by a similar mechanism in other grains as well, suggesting that this is a rather general mechanism for switching in a polycrystal.

To analyze the energetic contributions to local domain switching, we determined the changes in the local energy densities in grain A as switching progressed. Figs. 6 and 7 show the contours of the change in electric and elastic energy density distributions, respectively, at different stages of the switching process. The difference in the energy densities is calculated with reference to the domain structure presented in Fig. 5(i). For example, Fig. 6(i) represents the distribution of the difference in electrical energy density between the domain structures presented in Fig. 5(ii) and (i); the darker the color of the contour, the higher the magnitude of energy density. The iteration steps were chosen to be identical to those presented in Fig. 5(ii)–(iv).

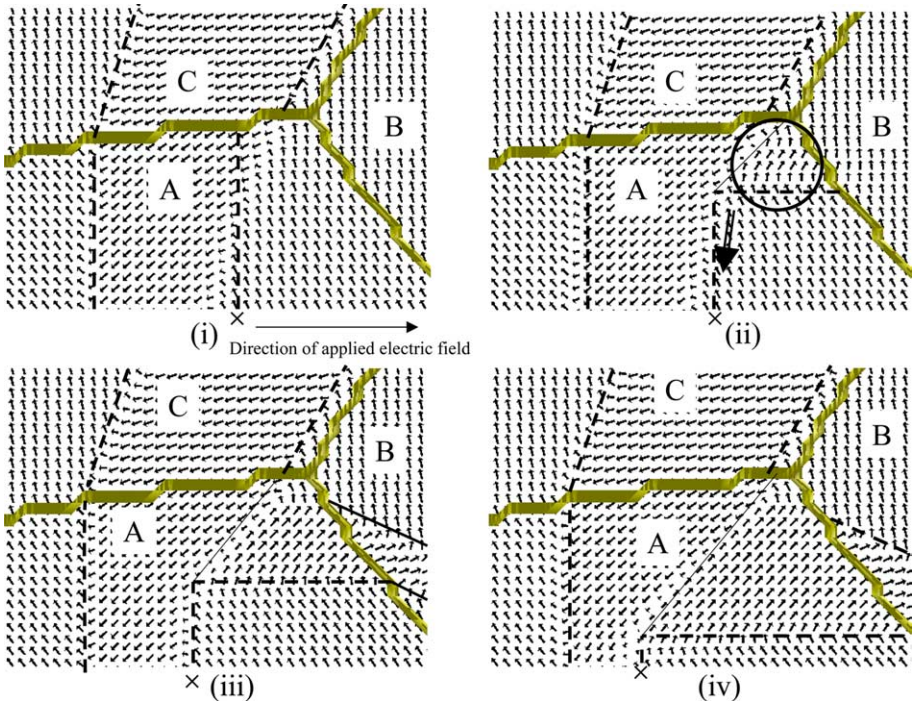

Fig. 5. Domain structure during switching at an applied electric field of $E_1 = 104.48$ kV/cm. Figures correspond to the point c in the PE loop of Fig. 3 at different iteration steps: (i) $N_{\text{itr}} = 1$; (ii) $N_{\text{itr}} = 500$; (iii) $N_{\text{itr}} = 1000$; (iv) $N_{\text{itr}} = 3700$. The filled lines represent grain boundaries, while the dashed and thin lines denote 90° and 180° domain walls, respectively. The nucleated 90° domain is marked by a circle. The big arrow shows the direction of growth of the nucleated 90° domain.

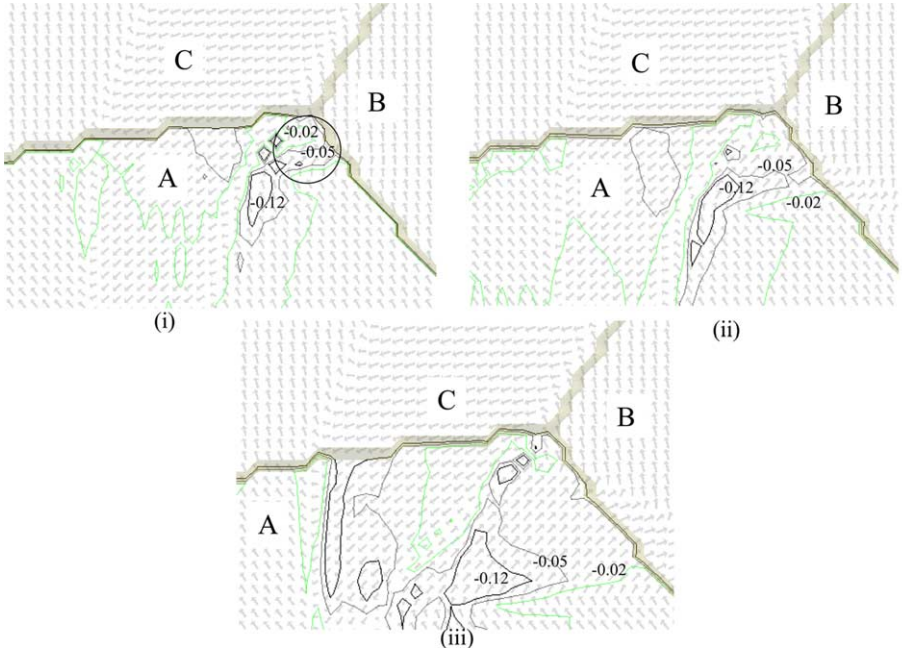

Fig. 6. Difference in electrical energy density of the domain structure presented in Fig. 5(ii)–(iv) with respect to that of the unswitched domain structure of Fig. 5(i).

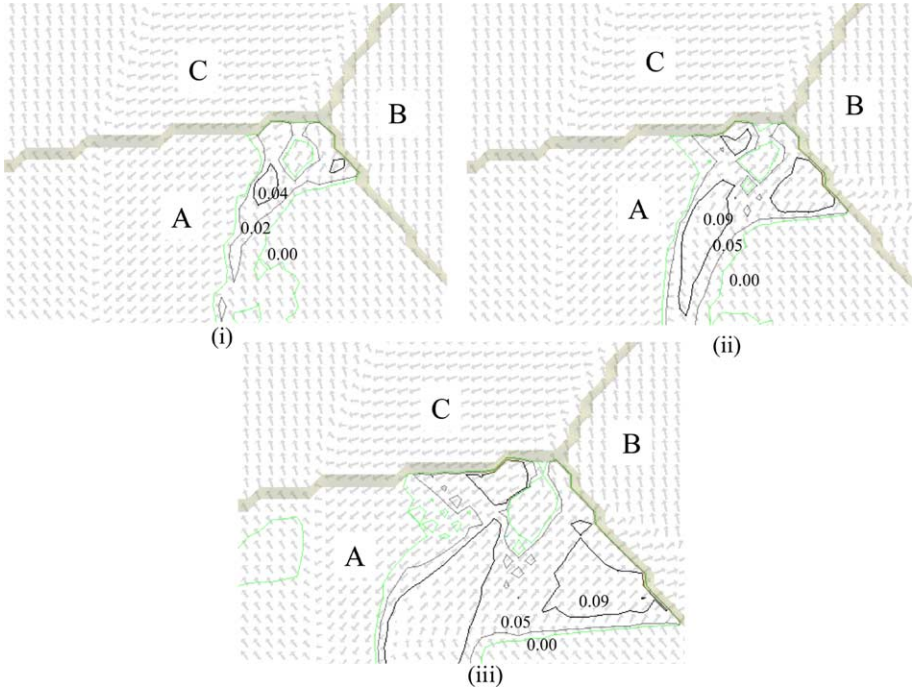

Fig. 7. Difference in elastic energy density of the domain structure presented in Fig. 5(ii)–(iv) with respect to that of the unswitched domain structure of Fig. 5(i).

5. Discussion

The stability of domain structures in ferroic materials is governed by competing energetic contributions. In the case of a ferroelectric material, the total energy includes the bulk free energy, domain wall energy, electrostatic energy, and elastic energy densities. Under an applied electric field, the changes in these energies determine the nucleation of a new domain at a particular site and growth by domain wall migration during polarization switching.

According to Fig. 6(i), the nucleation of a new domain near the grain boundary in grain A reduces the

electrical energy density locally. The figure shows that the nucleated domain marked by the circle is bounded by contour lines of −0.05 and −0.02. Fig. 6(ii)–(iii) illustrate how the growth of the 90° domains is also accompanied by a decrease in the electrical energy density with respect to the unswitched energy state. The decrease in electrical energy density during nucleation and growth can be attributed to the difference in polarization direction across the grain boundary between grains A and B. Nucleation and growth of a 90° domain in grain A helps to maintain a head-to-tail configuration across the grain boundary. The switching in grain A seems to promote the nucleation of a 90° domain within grain B near the grain boundary, indicating that switching in one grain influences the occurrence of switching in neighboring grains.

The elastic energy density changes during switching are shown in Fig. 7(i)–(iii). All contour lines near the switched domain have positive values, indicating that switching increases the elastic energy density locally compared to the unswitched state. Comparing Figs. 6 and 7, we conclude that the switching-induced increase in elastic energy density is more than offset by the decrease in electrical energy density; hence, the total energy density of the system decreases. Therefore, it can be concluded that nucleation and growth of 90° domains is primarily driven by the decrease in the electrical energy density.

Our observation of polarization switching by nucleation and growth of 90° domains has already been found in experiment. For example, Chen et al. [27] observed that polarization switching in PZT thin films occurs by nucleation of new 90° domains and subsequent growth of the nucleated domains. This confirms the behavior seen in Fig. 5(ii) that a new 90° domain nucleates at the twin boundary in grain A and grows toward the center of the grain along the twin boundary marked by the large arrow. Using a finite element model, Hwang et al. [11] suggested that the change in dielectric interaction energy arising from neighboring grains was the primary cause for 90° switching in ferroelectric polycrystals. In addition, our prediction that the polarization switching in one grain is facilitated by the polarization switching in a neighboring grain is consistent with prior observations by Cao et al. [28], which indicated that the domain switching process involves both intergranular and trans-granular cooperation.

It should be noted that our model takes into account the complicated local elastic and electrostatic interactions between neighboring grains that are present during polarization switching. Although the emphasis of this paper is on the domain switching mechanisms under an electric field, the model can be applied to domain evolution under an applied stress or to the simultaneous application of stress and an electric field. Furthermore, the present model can be applied directly to switching and domain evolution in a 3D system; as a matter of fact, a parallel version of the current computer code is being developed for the study of domain switching mechanisms and hysteresis loops in 3D. Moreover, it is possible to introduce other defects into the model, such as inhomogeneous compositional distributions, dislocations and second-phase precipitates [29–31]. Finally, in this work we assumed that the elastic coefficients are homogenous and isotopic, although real polycrystalline materials are always inhomogeneous. Numerical algorithms are now available [30,32] for taking elastic inhomogeneity into account, and its effect on ferroelectric domain switching will be the focus of future publications.

6. Conclusion

A 3D phase-field model has been developed for predicting domain structure evolution under an applied electric field in ferroelectric polycrystals. Based on the simulation of ferroelectric domain evolution, it was found that polarization reversal takes place by the nucleation and migration of 90° domain walls instead of by direct 180° domain switching. It was observed that these 90° domains nucleate at the grain boundaries and then grow toward the grain interior. The electrical energy was found to be the main driving force for both the nucleation and growth of 90° domains. Finally, it was demonstrated that polarization switching between neighboring grains is correlated.

Acknowledgements

Financial support from NSF under DMR-0122638 and DMR-0103354 is gratefully acknowledged.

References

[1] Lehnen P, Dec J, Kleemann W. J Phys D 2000;33:1932.
[2] Newnham RE, Xu QC, Kumar S, Cross LE. Ferroelectrics 1990;102:259.
[3] Merz WJ. Phys Rev 1954;95:690.
[4] Merz WJ. J Appl Phys 1956;27:938.
[5] Fatuzzo E. Phys Rev 1962;127:2036.
[6] Miller RC. J Phys Chem Solids 1960;17:93.
[7] Hu HL, Chen LQ. J Am Ceram Soc 1998;81:492.
[8] Ahluwalia R, Cao WW. Phys Rev B 2001;63:012103.
[9] Wang J, Shi SQ, Chen LQ, Li YL, Zhang TY. Acta Mater 2004;52:749.
[10] Li YL, Hu SY, Liu ZK, Chen LQ. Acta Mater 2002;50:395.
[11] Hwang SC, Arlt G. J Appl Phys 2000;87:869.
[12] Hwang SC, McMeeking RM. Int J Solids Struct 1999;36:1541.
[13] Arlt G. Ferroelectrics 1996;189:91.
[14] Zhang W, Bhattacharya K. Acta Mater 2005;53:185.
[15] Zhang W, Bhattacharya K. Acta Mater 2005;53:199.
[16] Jin YM, Artemev A, Khachaturyan AG. Acta Mater 2001;49:2309.

[17] Boettinger WJ, Warren JA, Beckermann C, Karma A. Ann Rev Mat Res 2002;32:163.
[18] Chen LQ. Ann Rev Mater Res 2002;32:113.
[19] Krill CE, Chen LQ. Acta Mater 2002;50:3057.
[20] Pertsev NA, Zembilgotov AG, Tagantsev AK. Phys Rev Lett 1998;80:1988.
[21] Goldstein H. Classical mechanics. Cambridge, MA: Addison-Wesley; 1953.
[22] Mura T. Micromechanics of defects in solids. The Hague: Martinus Nijhoff; 1982.
[23] Tilley DR. Ferroelectric Ceramics. Boston, MA: Birkhauser; 1993.
[24] Chen LQ, Shen J. Comp Phys Commun 1998;108:147.
[25] Haun MJ, Furman E, Jang SJ, McKinstry HA, Cross LE. J Appl Phys 1987;62:3331.
[26] Stemmer S, Streiffer SK, Ernst F, Ruhle M, Hsu WY, Raj R. Solid State Ionics 1995;75:43.
[27] Chen L, Ouyang Q, Ganpule CS, Nagarajan V, Ramesh R, Roytburd AL. Appl Phys Lett 2004;84:254.
[28] Cao W, Randall CA. J Phys Chem Solids 1996;57:1499.
[29] Hu SY, Li YL, Chen LQ. J Appl Phys 2003;94:2542.
[30] Wang YU, Jin YMM, Khachaturyan AG. J Appl Phys 2002;92:1351.
[31] Zhu JZ, Wang T, Ardell AJ, Zhou SH, Liu ZK, Chen LQ. Acta Mater 2004;52:2837.
[32] Hu SY, Chen LQ. Acta Mater 2001;49:1879.